Journal of Porous Materials (2022) 29:1991–2001
https://doi.org/10.1007/s10934-022-01313-2

Facile hydrothermal synthesis of NiO/rGO nanocomposite electrodes for supercapacitor and nonenzymatic glucose biosensing application

O. C. Pore[1,2] · A. V. Fulari[3] · V. G. Parale[4] · H. H. Park[4] · R. V. Shejwal[1] · V. J. Fulari[2] · G. M. Lohar[1]

Accepted: 16 July 2022 / Published online: 1 August 2022

Abstract
The NiO/rGO composites are synthesized via a hydrothermal method followed by annealing treatment with varying graphene oxide concentrations. The structural and morphological characterizations of synthesized samples are done by XRD, FT-IR, Raman, and FE-SEM. The electrochemical supercapacitor performance of prepared electrodes is characterized by CV, GCD, and EIS studies. The NiO/rGO composite achieved the highest specific capacitance of 727.1 F g^{-1} at 1 mA cm^{-2} current density and showed good cyclic stability of about 80.4% over 9000 cycles. In a nonenzymatic glucose sensing study, the sensing properties are analyzed by CV and chronoamperometry. The NiO/rGO composite showed the highest glucose sensitivity of 442.4 µA mM^{-1} cm^{-2} with correlation coefficient $R^2 = 0.9964$ and LOD of 7.42 µM.

Keywords NiO · rGO · Hydrothermal · Supercapacitor · Glucose biosensing

1 Introduction

The environmental issues and energy crises caused by high energy demand have attracted researchers' attention to the development and utilization of eco-friendly and renewable energy sources [1–3]. Supercapacitors are promising and noteworthy energy storage devices because of their rapid charging and discharging rates, high energy and power densities, long cyclic lifetime, wide operating temperature, and operational safety [4–6]. Supercapacitors are of two types: electric double-layer capacitors (EDLCs) with nonfaradic charge storage and pseudocapacitors with the faradic mechanism. Carbon-based nanomaterials and their derivatives having high surface area as well as electrical conductivity, such as carbon nanotubes (CNT), activated carbon, graphene, etc., show EDLC-type behavior. Even though EDLCs show high electrical conductivity, they suffer from low specific capacitance [7–10]. The transition metal hydroxides, metal oxides such as $Ni(OH)_2$, $Co(OH)_2$, V_2O_5, RuO_2, NiO, MnO_2, Co_3O_4, etc., and conducting polymers are used for pseudocapacitors. The promising properties of NiO, such as environmental friendliness, low cost, high thermal and chemical stability, high thermotical capacities, etc., make NiO a promising electrode material for supercapacitor application [11].

Nevertheless, despite these promising properties, NiO electrodes still exhibited challenges such as poor electrical conductivity, which leads to poor rate capabilities and low specific capacitance (sp. capacitance) as capered to the theoretical value, etc. [12]. To transcend the limitation of poor electrical conductivity of NiO, one of the effective strategies is the introduction of carbon-based materials such as CNT, graphene, acetylene black, etc., in NiO, which helps improve its electrical conductivity [13, 14]. Xu et al. [11] synthesized NiO/rGO using a simple hydrothermal route. The prepared NiO/rGO electrode achieved a sp. capacitance of 171.3 F g^{-1} at 0.5 A g^{-1}. Also, it shows 79% cyclic stability over 2000 cycles. Huang et al. [15] fabricated NiO-graphene hybrid film through a series of controlled fabrication processes. The synthesized NiO-graphene film shows 540 F g^{-1} sp. capacitance at 2 A g^{-1}. Also, it exhibited about 80% capacity retention over 2000 cycles. Bu et al. [16] developed NiO/rGO composite electrodes via a one-pot chemical reduction

✉ G. M. Lohar
gauravlohar24@gmail.com

1 Department of Physics, Lal Bahadur Shastri College of Arts, Science and Commerce, Satara 415002, India

2 Department of Physics, Holography and Materials Research Laboratory, Department of Physics, Shivaji University, Kolhapur, Maharastra 416004, India

3 Division of Physics and Semiconductor Science, Dongguk University, Seoul 04620, South Korea

4 Department of Materials Science and Engineering, Yonsei University, Seoul 03722, Republic of Korea

method, which achieved a capacitance of 461 F $g^{-}1$ at 0.21 A g^{-1}. Kumar et al. [17] synthesized NiO@rGO nanocomposite via microwave irradiation method exhibited 395 F g^{-1} sp. capacitance at 1 A g^{-1}. Yus et al. [18] synthesized core–shell rGO-NiO nanostructures using an electrophoretic deposition method. The hybrid electrode shows a 940 F g^{-1} capacitance at 2 A g^{-1}.

Glucose act as a source of energy for the human body. However, excess consumption of glucose in the human body leads to diabetes. Diabetes in a few cases may cause other diseases like Kidney failure, blindness, and heart failure [19, 20]. Hence, glucose measurement is necessary for the diagnosis of diabetes and biotechnology, pharmaceutical industries, food industries, etc. [21, 22]. The electrochemical glucose sensor is a powerful method for detecting glucose as it is simple, cost-effective, and susceptible. NiO nanostructures play an important role in enzymeless glucose-sensing because of their $Ni(OH)_2$/NiOOH redox reactions in a NaOH solution [23]. Also, it is known that carbon-based materials have a positive impact on the enhancement of detection performance of electrochemical sensors [24–30]. Zhang et al. [31] synthesized Nanoparticles-assembled NiO nanosheets with GO film as a template by a two-step calcination method. The synthesized glucose sensor exhibited 1138 µA mM^{-1} cm^{-2} sensitivity. Lu et al. [32] synthesized a nonenzymatic glucose sensor based on NiO/RGO and developed it by the ultrasonic co-assembly method. The prepared electrode shows the maximum sensitivity of 3796 µA mM^{-1} cm^{-2}. Huang et al. [14] synthesized three-dimensional NiO hollow spheres/rGO composite exhibited the highest 2.04 mA mM^{-1} cm^{-2} glucose sensitivity.

In the present work, NiO/rGO composite by varying GO concentration are prepared via a simple hydrothermal method. The NiO/rGO composite with 120 mg GO shows 727.1 F g^{-1} sp. capacitance at 1 mA cm^{-2}. Also, it exhibited good cyclic stability of about 80.4% after 9000 cycles at 7 mA cm^{-2} current density. The NiO/rGO composite with 120 mg GO revealed a maximum glucose sensitivity of 442.4 µA mM^{-1} cm^{-2} compared to other electrodes with $R^2 = 0.9964$ and a limit of detection (LOD) of 7.42 µM.

2 Materials and methods

2.1 Chemicals

All the chemicals used in this study were analytical grade and used without further purification. Nickel chloride hexahydrate [$NiCl_2 \cdot 6H_2O$] (99%), Urea [$CO(NH_2)_2$] (99%), Sulphuric Acid [H_2SO_4] (98%), Potassium permanganate [$KMnO_4$] (99%), Hydrogen Peroxide [H_2O_2] (30%), Potassium hydroxide [KOH] (85%), Sodium hydroxide [NaOH] (98%) and Hydrochloric acid [HCl] (35.4%), were obtained from Thomas Baker India Pvt. Ltd. (Mumbai, India). Polyvinylidene Fluoride [PVDF] (Battery grade), 1-Methyl-2-pyrrolidinone [NMP] (99%), and graphite powder (< 20 µm) were obtained from Sigma Aldrich India.

2.2 Synthesis of NiO/rGO composites

The GO was prepared by using the modified Hummers method using the previously reported process [33]. The NiO/rGO nanostructures by varying GO concentrations were prepared by hydrothermal route. In the fabrication of NiO/rGO, 7.131 g of $NiCl_2 \cdot 6H_2O$ and 3.6036 g $CO(NH_2)_2$ were added to 60 mL of double-distilled water (DDW). Different amounts of GO powder (0, 60, 120, and 180 mg) were added in 30 mL DDW in a separate beaker and ultrasonicated for 1 h. Then, these solutions were mixed and kept on constant stirring for 1 h. The obtained homogeneous solution was transferred into a Teflon liner, sealed in the autoclave, and maintained at 150 °C for 6 h. Afterward, the product was cleaned with DDW and ethanol many times and dried at 60 °C for 12 h. Lastly, the resulted powders were annealed at 400 °C for 2 h. Based on GO concentration, the resulting powders were named NG-0, NG-60, NG-120, and NG-180, respectively. The formation of different NiO/rGO composites (NG-0, NG-60, NG-120, and NG-180) is shown in Scheme 1**.** The working electrodes were prepared on the copper foil (CF) as a current collector as explained in previous literature [19]. The electrodes prepared on CF as current collector by using NG-0, NG-60, NG-120, and NG-180 powders were named as N1G-0, N2G-60, N3G-120, and N4G-180 electrodes respectively.

2.3 Characterization of materials

The structural characterizations of the prepared sample were characterized using an X-ray diffractometer (XRD, Rigaku Ultima, Japan) with Cu Kα (λ = 0.154 nm) radiation. Fourier transform-infrared spectrometry (FT-IR, Lambda-7600, Australia) to detect functional groups in the prepared material. The micro-Raman (LabRam Aramis, Horiba Jobin Yvon, France) spectrometer was used to record Raman spectra of samples. A Thermoscientific ESCALAB 250 (Thermo Fisher Scientific, UK) instrument was used for X-ray photoelectron spectroscopy (XPS) measurement. Field emission scanning electron microscopy (FE-SEM, Mira-3, Tescan Pvt. Brno-Czech Republic) was used to investigate the morphology of material and Energy dispersive spectrometer (EDS, Oxford Instrumentations inbuilt with FE-SEM) for elemental analysis.

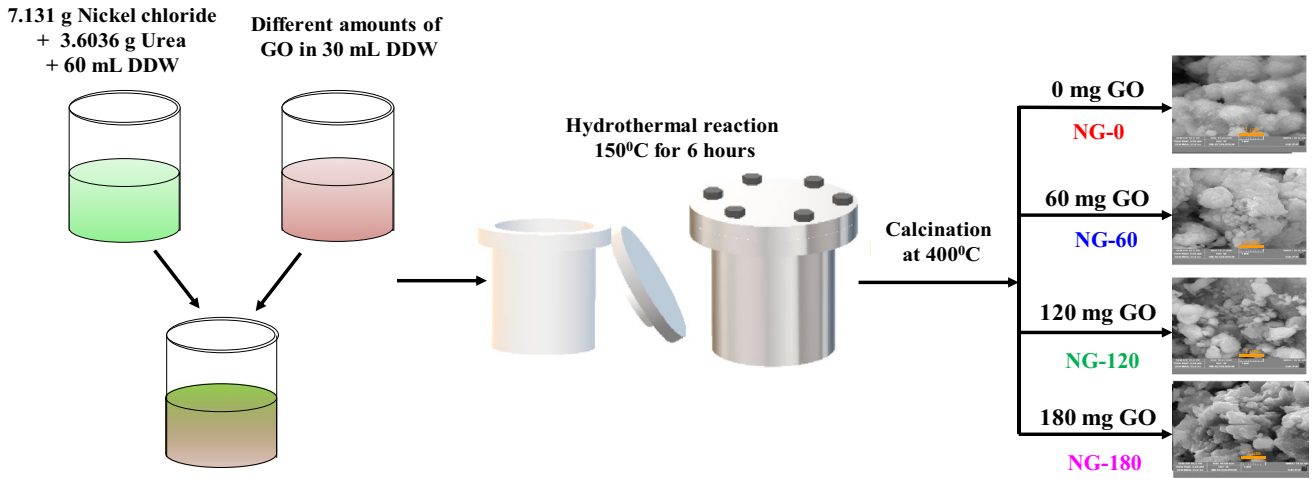

Scheme 1 Schematic presentation of synthesis of different NiO/rGO powders by hydrothermal method

2.4 Electrochemical measurements

All the electrochemical measurements of working electrodes in the supercapacitor and glucose sensing study were done in a three-electrode system at ambient conditions. In the three-electrode system prepared electrodes were used as working electrodes, saturated calomel electrode as reference electrode, and platinum wire as counter electrode respectively. The cyclic voltammetry (CV), GCD, electrochemical impedance spectroscopy (EIS), and chronoamperometry (CA) study of the sample was done by an electrochemical workstation (Biologic SP-300, Spain).

3 Results and discussion

3.1 FTIR study

The FTIR study of NiO/rGO powders synthesized by varying GO concentrations (NG-0, NG-60, NG-120, and NG-180) is presented in Fig. 1A. The peaks observed at 3450 cm^{-1} were attributed to hydroxyl groups of absorbed water [34]. The peak observed at about 1625 cm^{-1} corresponded to the C = C bonds. The peaks observed at about, 1398, 1227, and 1063 cm^{-1} are attributed to, C–C, C-O, and C–O–C bonds [35–37]. The absorption peaks between 400 and 500 and 660 cm^{-1} are assigned to the stretching vibrations of Ni–O [19, 38, 39]. The fading of a peak at 1723 cm^{-1} ascribed to the C = O in NG-60, NG-120, and NG-180 powders is due to the reduction of GO to rGO [37].

3.2 XRD study

The XRD spectrum of each sample was recorded to investigate the crystal structure of synthesized NiO/rGO powders. Figure 1B presents the XRD spectra of NiO/rGO powders. The XRD diffraction peaks of NG-0, NG-60, NG-120, and NG-180 powders correspond with JCPDS card: 00-047-1049. The diffraction peaks of NG-0, NG-60, NG-120, and NG-180 powders at 37.06°, 43.26°, 62.78°, and 75.50° are attributed to the (111), (200), (220), and (311) crystal planes of NiO respectively. The Debye Scherrer formula was used to calculate crystallite size [40]. The estimated crystallite size for NG-0, NG-60, NG-120, and NG-180 powders corresponding to the (200) plane is 11.86, 25.45, 25.43, and 35.61 nm. The characteristic peak of rGO at about 25° in powder NG-60, NG-120, and NG-180 is not present, which may probably be because of signal converging by NiO. So, the rGO in the composite is confirmed by Raman spectra.

3.3 Raman spectra

Figure 1C illustrates the Raman spectra of different NiO/rGO composites (NG-0, NG-60, NG-120, and NG-180). The absorption peak in Fig. 1C at around 511 cm^{-1} for NG-0, NG-60, NG-120, and NG-180 samples correspond to the first-order longitudinal optical (LO) mode, while the peak at 1063 cm^{-1} indicates 2LO phonon mode of Ni–O bond [14]. The peaks at about 1355 and 1597 cm^{-1} in the NG-60, NG-120, and NG-180 indicate the D band (because of defected carbon layer) and G band (due to the second-order scattering of the graphitic carbon) respectively [41]. The D band of GO, NG-60, NG-120, and NG-180 are at about 1350, 1317, 1355, 1352 cm^{-1}, while the G band is at about 1609, 1568, 1597, and 1591 cm^{-1} respectively. The shift of the G and D band positions of NG-60, NG-120, and NG-180 as compared to GO indicates the reduction of GO in NiO/rGO composites during the hydrothermal process [42].

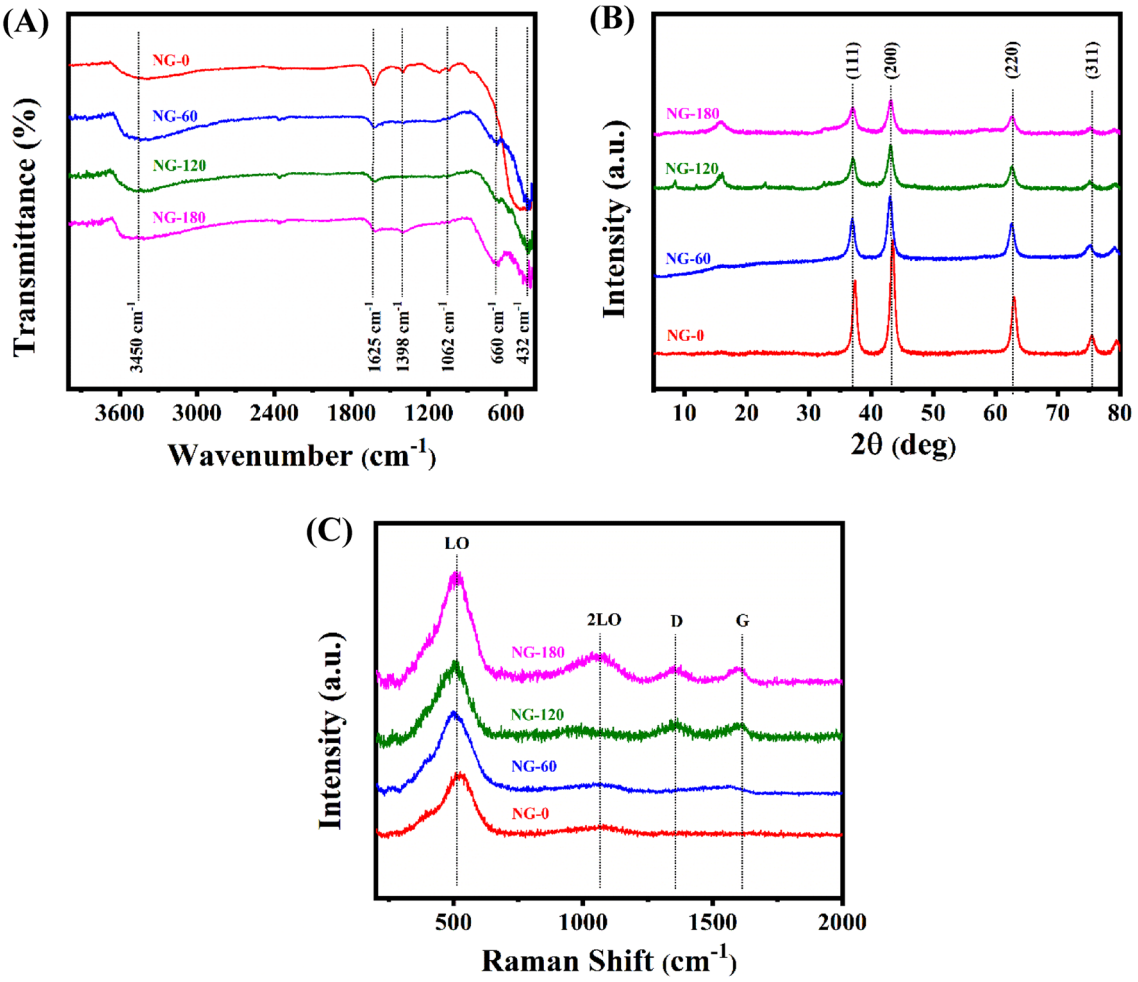

Fig. 1 Structural characterizations **A** FT-IR, **B** XRD, and **C** Raman study of different NiO/rGO powders (NG-0, NG-60, NG-120, and NG-180)

3.4 XPS spectra

Figure 2A shows the survey spectrum of NG-120 powder and designates the presence of Nickel, oxygen, and carbon elements. The observed peaks of Ni 2p, O 1 s, and C 1 s reveal the existence of NiO and rGO in the NG-120 powder. In Ni 2p spectrum (Fig. 2B), the main peaks observed at 854.7 as well as 872.1 eV can be ascribed to the $2p_{3/2}$ and $2p_{1/2}$ spin-orbits of NiO while their corresponding satellites are present at 860.3 eV and 878.1 eV, respectively [14]. As shown in Fig. 2C the peaks at 284.1, 285.6, and 287.7 eV are related to the C = C, C–OH (epoxy/hydroxy), and O–C = O (carboxyl) respectively [43]. The peaks located at 530.9 and 528.5 eV in the O 1 s spectrum Fig. 2D are related to C = O/Ni–O and O-Ni/C-O-Ni bonding configurations, respectively [42, 44].

3.5 FE-SEM study

Figure 3A–D presents the FE-SEM images of different NiO/rGO composites (NG-0, NG-60, NG-120, and NG-180). The bare NiO, i.e., NG-0 powder, shows the urchinlike structure [19]. After the addition of GO in NiO, the urchinlike structure is observed to disappear in NG-60, NG-120, and NG-180 samples. This may be because the urchinlike NiO nanostructures get covered with rGO sheets. The rGO sheets are uniformly dispersed on the surface of NiO nanostructures. This disappearance of spikes of urchinlike NiO because of rGO wrapping also shows that the rGO is tightly compounded with NiO. Such rGO sheets act as conducting networks and help improve electrochemical supercapacitor and nonenzymatic glucose sensing performance. In the case of supercapacitor application, rGO also serves as good

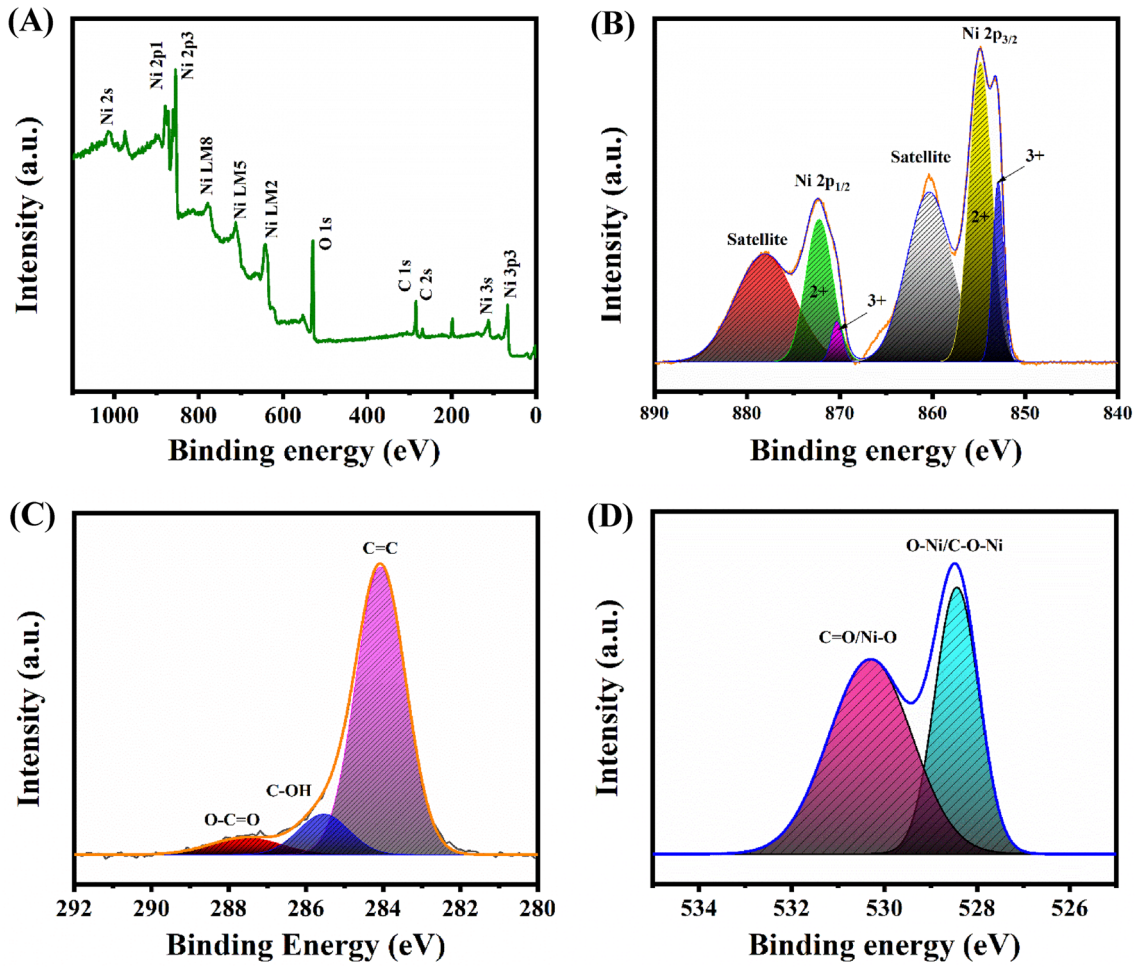

Fig. 2 XPS analysis **A** survey spectrum of NG-120 sample, **B** Ni 2p, **C** C 1 s, and **D** O 1 s

EDLC material and helps to enhance electrochemical performance. Figure 3E presents the EDS spectra of the NG-120 sample. The presence of nickel, oxygen, and carbon in the EDS spectrum confirms the presence of NiO and rGO.

3.6 EIS study

Three electrode system was employed to study supercapacitor performance. The Nyquist plots of N1G-0, N2G-60, N3G-120, and N4G-180 electrodes are depicted in Fig. 4A. The Nyquist plots were taken in the 0.1 Hz–100 kHz frequency range. The inset of Fig. 4A presents the equivalent circuit diagram. The solution resistance (R_s) values for N1G-0, N2G-60, N3G-120 and N4G-180 electrodes are 1.79, 1.42, 1.25, and 1.73 Ω cm^{-2} respectively. The lower value of R_s suggests the better electrode material's attachment to the CF. In case of N4G-180 electrode with higher rGO content than N3G-120 electrode, the increase in R_s value is observed. This may be because of inconvenient agglomeration of Co_3O_4 with rGO sheets, leads to a reduction in active surface area and active sites for redox reactions in N4G-180 electrode [45]. The Bode plots of N1G-0, N2G-60, N3G-120, and N4G-180 samples are presented in Fig. 4B.

3.7 Supercapacitor study

The supercapacitor performance of all electrodes was done in a 1.0 M KOH electrolyte. The CVs of all NiO/rGO electrodes at 5 mV s^{-1} are shown in Fig. 5A. The CVs of NiO/rGO electrodes are more significant as compared to bare NiO electrodes. This is because rGO in NiO/rGO composite offers more active sites responsible for redox reactions than bare NiO and improves its conductivity. The redox reactions of OH^- with remaining functional groups of rGO contribute to redox reactions in NiO/rGO composites. The comparative GCD curves of N1G-0, N2G-60, N3G-120, and N4G-180 electrodes at a 1 mA cm^{-2} current density are shown in Fig. 5B. From GCD curves, it is observed that the NiO/rGO composites, i.e., N2G-60, N3G-120, and N4G-180 electrodes, show better discharge

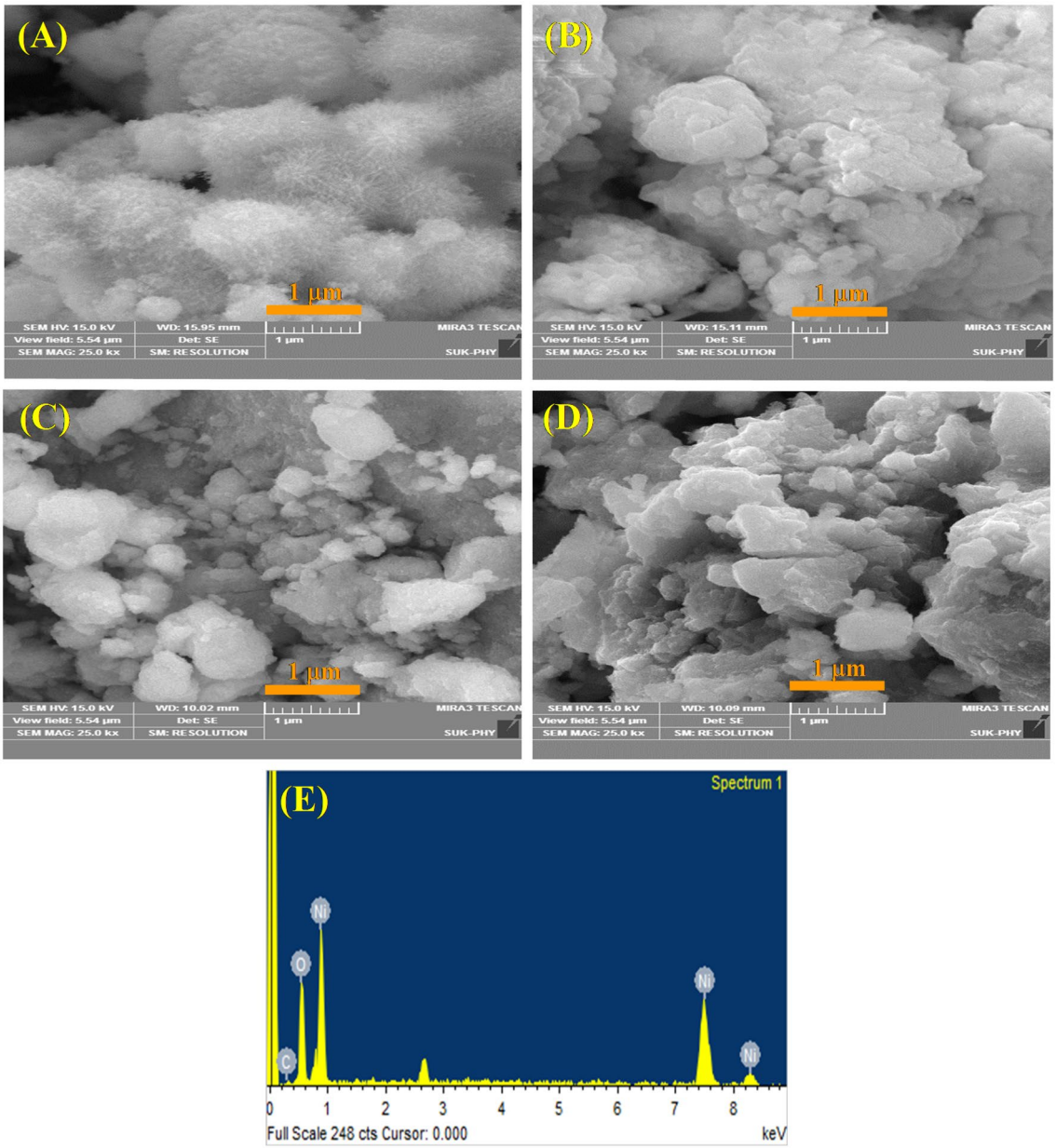

Fig. 3 FE-SEM micrographs of **A** NG-0, **B** NG-60, **C** NG-120, and **D** NG-180 powders **E** EDS pattern of NG-120

time as compared to bare NiO, i.e., N1G-0 electrode. This is because the rGO enhances the conductivity and provides more active sites for the redox reaction responsible for charge and discharge. Figure 5C presents the sp. capacitance of all electrodes at (1 to 5 mA cm^{-2}) current densities. The maximum sp. capacitance calculated from GCD for N1G-0, N2G-60, N3G-120, and N4G-180 electrodes is 246.6, 384.7, 727.1, and 349.4 F g^{-1}, respectively. Figure 5 (D) presents the Regone plot of all NiO/rGO electrodes. The N3G-120 electrode shows the maximum 16.16 Wh kg^{-1} energy density at an 86.96 W kg^{-1} power density. Stability is one of the essential parameters in supercapacitor study. Figure 5E presents the cyclic stability of the optimized N3G-120 electrode at 7 mA cm^{-2} current density. The N3G-120 electrode exhibited good cyclic stability of about 80.4% after 9000 cycles. Figure 5F shows the first five (blue) and last five (red) GCD cycles of 9000 cycles. The better supercapacitor performance of N3G-120 electrodes is credited to both NiO and rGO where the high conductivity of rGO helps to enhance the electrical conductivity of the NiO/rGO composite. Such high conductivity is also responsible for better cyclic performance. The comparative supercapacitor study is mentioned in Table 1.

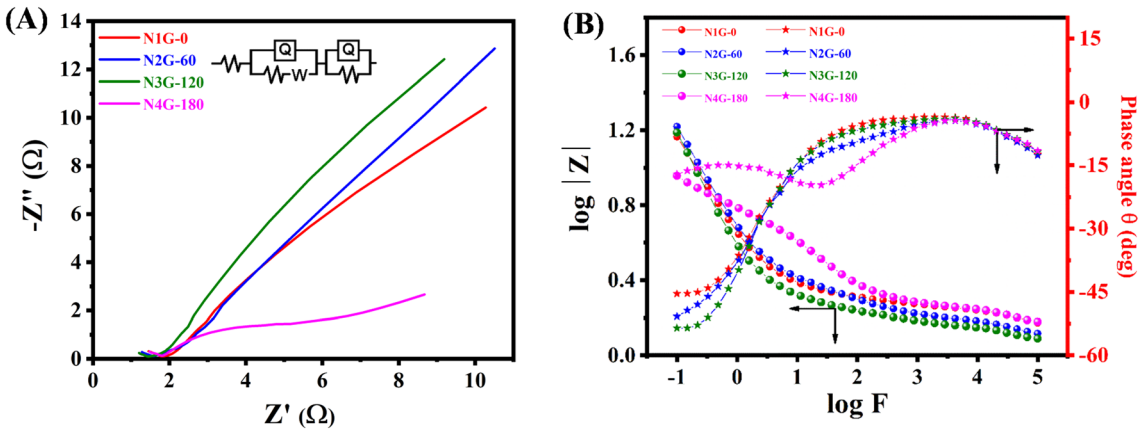

Fig. 4 Electrochemical impedance spectroscopy study **A** Nyquist plot, **B** Bode plot of N1G-0, N2G-60, N3G-120, and N4G-180 electrodes

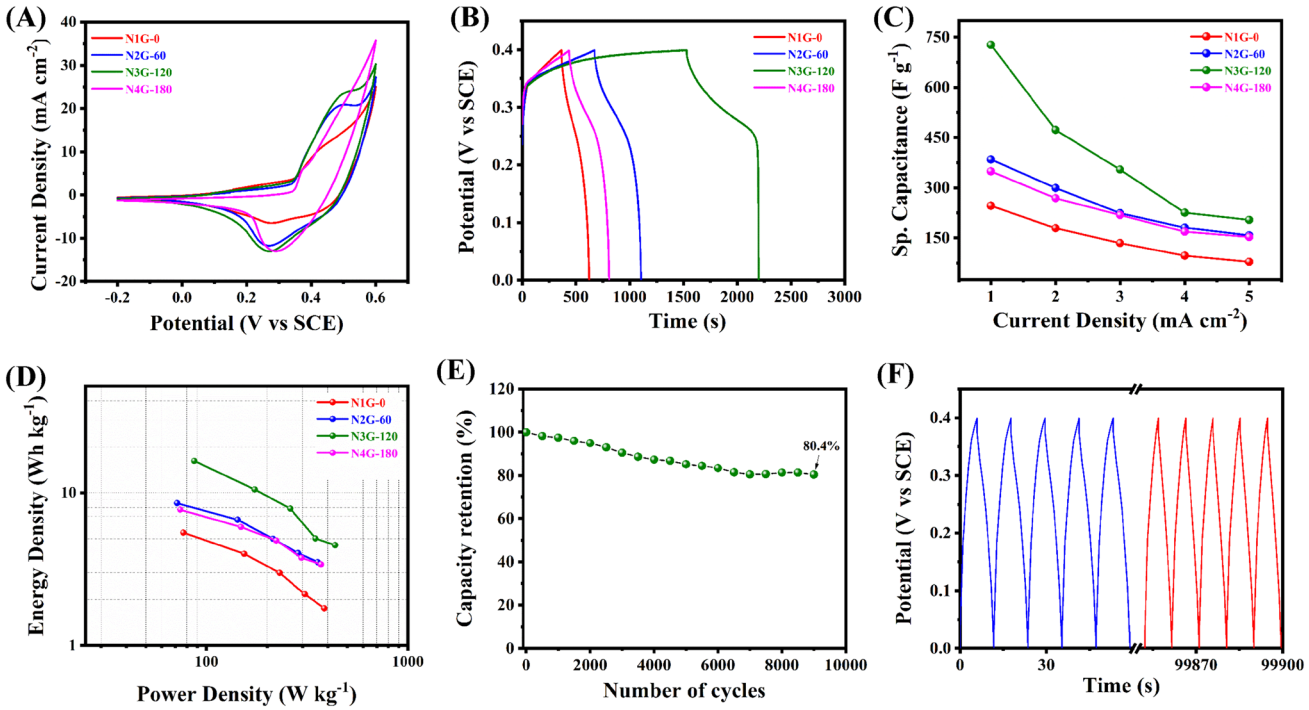

Fig. 5 Supercapacitor performance of NiO/rGO. **A** The CV curves of N1G-0, N2G-60, N3G-120, and N4G-180 electrodes at 5 mV s^{-1}. **B** The comparison of GCD cycles of N1G-0, N2G-60, N3G-120, and N4G-180 electrodes at 1 mA cm^{-2}. **C** sp. capacitance calculated from GCD cycles of N1G-0, N2G-60, N3G-120, and N4G-180 electrodes vs. current density. **D** Regone plot of N1G-0, N2G-60, N3G-120, and N4G-180 electrodes. **E** Cyclic stability of N3G-120 electrode over 9000 charging-discharging cycles. **F** First and last five GCD cycles of cyclic stability

3.8 Nonenzymatic glucose biosensing study

The electrolyte used in the glucose-sensing experiment was 0.1 M NaOH. Figure 6A–D depicts the CVs of electrodes N1G-0, N2G-60, N3G-120, and N4G-180 without glucose (blue) and with 3 mM glucose (red). After the addition of 3 mM glucose, all electrodes show an increase in the current response. Figure 6E–H shows the CVs of N1G-0, N2G-60, N3G-120, and N4G-180 electrodes after the addition of different concentrations of glucose. After the addition of glucose, all electrodes show a linear increase in CVs. The mechanism of NiO glucose oxidation is as follows: [14]

$$NiO + OH^- \rightarrow NiOOH + e^-$$

Table 1 Comparison of supercapacitor performance of our prepared electrode with other published NiO/rGO-based materials

Sr. no	Electrode material	Current collector	Electrolyte	Sp. capacitance (F g^{-1})	Cyclic stability	References
1	NiO–rGO	GCE	6 M KOH	171.3 (0.5 A g^{-1})	79.07% after 2000 cycles	[11]
2	NiO-graphene	Ni Foil	2 M KOH	540 (2 A g^{-1})	80% after 2000 cycles	[15]
3	NiO/rGO	Ni Foam	6 M KOH	461 (0.21 A g^{-1})	74.5% after 5000 cycles	[16]
4	NiO@rGO	Ni Foam	6 M KOH	395 (1 A g^{-1})	–	[17]
5	rGO/NiO	Ni Foam	1 M KOH	940 (2 A g^{-1})	–	[18]
6	NiO/rGO	Ni Foam	6 M KOH	428 (0.48 F g^{-1})	90% after 5000 cycles	[49]
7	NiO-rGOH	–	2 M KOH	351 (0.625 A g^{-1})	91% after 1000 cycles	[50]
8	NiO/rGO	Ni Foam	6 M KOH	950 (1 A g^{-1})	91.3% after 1000 cycles	[51]
9	NiO-Graphene	Graphite	1 M KOH	500 (5 V s^{-1})	84% after 3000 cycles	[52]
10	NiO/rGO	CF	1 M KOH	727.1 (1 mA cm^{-2})	80.4% after 9000 cycles	This Work

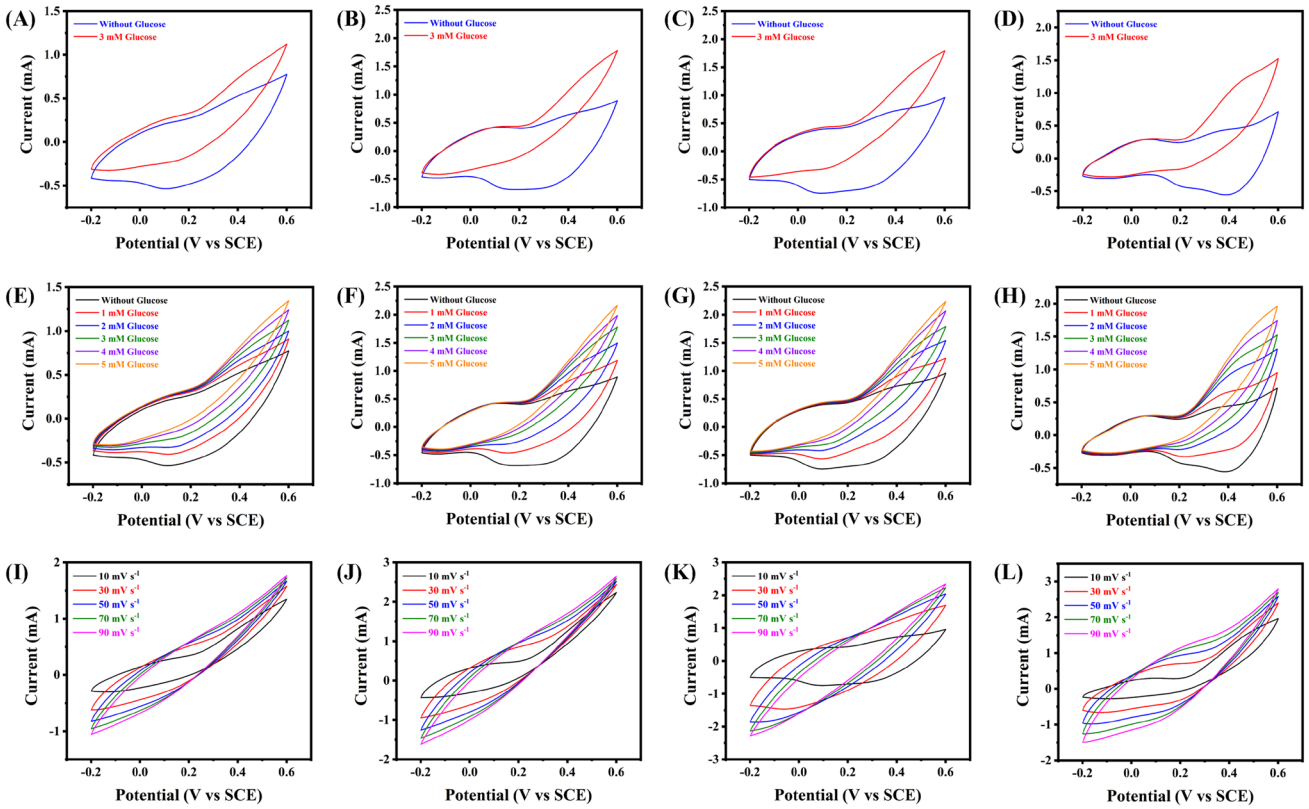

Fig. 6 **A–D** CVs without glucose (blue) and with 3 mM glucose (red) of N1G-0, N2G-60, N3G-120, and N4G-180 electrodes, respectively at 10 mV s^{-1} scan rate. **E–H** CVs of N1G-0, N2G-60, N3G-120, and N4G-180 electrodes respectively at different concentrations of glucose (0 to 5 mM). **I–L** CVs of N1G-0, N2G-60, N3G-120, and N4G-180 electrodes at different scan rates (Color figure online)

$$NiOOH + glucose \rightarrow NiO + glucolactone$$

The increased current response in CV after the addition of glucose is because of the electrooxidation of glucose with NiO, accompanied by oxidation from Ni^{2+} to Ni^{3+} [14]. Figure 6I–L depicts the CVs of N1G-0, N2G-60, N3G-120, and N4G-180 electrodes at (10–90 mV s^{-1}) scan rates respectively in the presence of 5 mM glucose.

The chronoamperometry (CA) technique is used in non-enzymatic glucose sensing to analyze glucose due to its high sensitivity [14, 46–48]. Figure 7A–D shows the CA responses of N1G-0, N2G-60, N3G-120, and N4G-180 electrodes at + 0.5 V potential at different concentrations

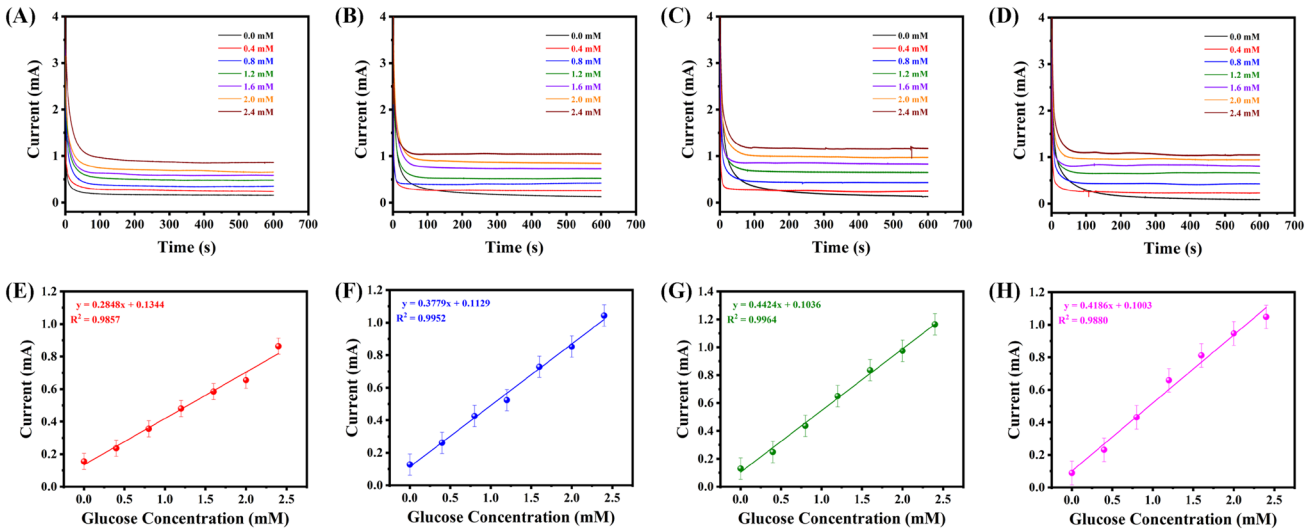

Fig. 7 **A**-**D** Chronoamperometric responses at + 0.50 V operating potential of N1G-0, N2G-60, N3G-120, and N4G-180 electrodes at different concentrations of glucose (0 to 2.4 mM) in 0.1 M NaOH solution. **E**–**H** The corresponding calibration graphs of N1G-0, N2G-60, N3G-120, and N4G-180 electrodes, respectively

of glucose (0 to 2.4 mM). From the observation of Fig. 7(A–D), it is clear that the current in the CA curve increases with increasing glucose concentration. The calibration curves of glucose concentration versus current observed for N1G-0, N2G-60, N3G-120, and N4G-180 electrodes are shown in Fig. 7E–H, respectively. All electrode shows linearity in the range of glucose concentration 0.4 to 2.4 mM. The electrode N3G-120 exhibited the highest 442.4 μA mM^{-1} cm^{-2} glucose sensitivity compared to other electrodes with $R^2 = 0.9964$ and LOD of 7.42 μM.

The conductivity of rGO further improves the conducting network in NiO/rGO composites and is responsible for better electron transfer kinetics. Hence NiO/rGO composite could provide more active sites for absorbing glucose and responsible for good sensitivity. Figure 8A–D shows the CA study of N1G-0, N2G-60, N3G-120, and N4G-180 electrodes obtained in the presence of glucose and relevant interfering species. The current responses of N1G-0, N2G-60, N3G-120, and N4G-180 electrodes with 1.0 mM glucose and common interferences such as 0.2 mM of Fructose, Ascorbic acid, NaCl, and KCl are shown in Fig. 8E–H

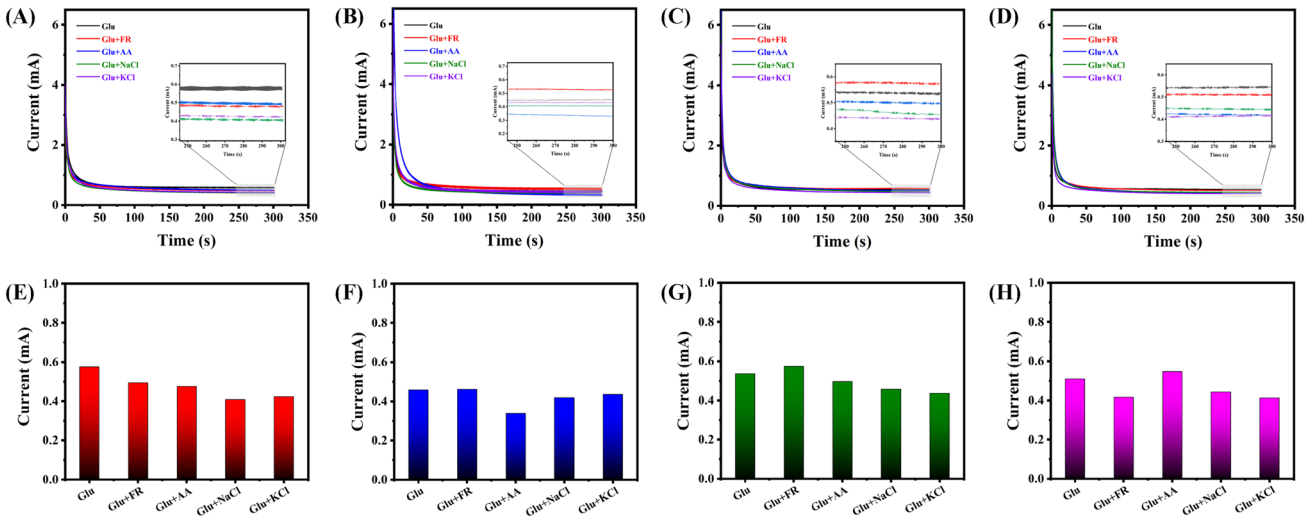

Fig. 8 **A**–**D** Chronoamperometric responses of N1G-0, N2G-60, N3G-120, and N4G-180 electrodes obtained in 1.0 mM glucose and different relevant interfering species (Inset: enlarged graph of current responses of respective electrodes in the presence of glucose and interfering species). **E**–**H** Bar diagram for the current responses with glucose and relevant interfering species

respectively. The N3G-120 electrode, as compared to the other electrodes, shows the minimum change in response towards glucose even in the presence of interfering species.

4 Conclusion

Herein, NiO/rGO composites are prepared by hydrothermal, followed by annealing treatment by varying GO concentrations. The NiO/rGO composite shows a highest of 727.1 F g^{-1} sp. capacitance at 1 mA cm^{-2}. Also, it exhibited good cyclic stability of about 80.4% after 9000 cycles. In the case of nonenzymatic glucose sensing, the optimized NiO/rGO composite exhibited the maximum 442.4 μA mM^{-1} cm^{-2} glucose sensitivity compared to other electrodes with $R^2 = 0.9964$ and LOD of 7.42 μM. The prepared electrode shows excellent electrochemical supercapacitor and nonenzymatic glucose biosensing properties.

Acknowledgements Dr. G. M. Lohar is thankful to DST-SERB, Government of India, for providing funds under the ECRA scheme File No: ECR/2017/002099.

Author contributions OCP: Methodology, Writing—original draft. AVF: Characterizations. VGP: Characterizations. HHP: Characterizations. RVS: Review. VJF: Review. GML: Conceptualization, Writing—review & editing.

Declarations

Competing interests The authors declare no competing interests.

Conflict of interest The authors declare that they have no known competing financial interests or personal relationships that could have appeared to influence the work reported in this paper. The authors declare the following financial interests/personal relationships which may be considered as potential competing interests

References

1. N.C. Maile, M. Moztahida, A.A. Ghani, M. Hussain, K. Tahir, B. Kim, S.K. Shinde, V.J. Fulari, D.S. Lee, Chem. Eng. J. **421**, 129767 (2021)
2. S.X. Yuan, M.H. Yang, C.X. Lu, X.M. Wang, New Carbon Mater. **35**, 731 (2020)
3. O.C. Pore, A.V. Fulari, R.V. Shejwal, V.J. Fulari, G.M. Lohar, Chem. Eng. J. **426**, 131544 (2021)
4. Q. Li, Q. Wei, L. Xie, C. Chen, Lu. Chunxiang, Su. Fang-Yuan, P. Zhou, RSC Adv. **6**, 46548 (2016)
5. S.R. Nikam, K. Shinde, D.P. Dubal, G.S. Ghodake, H.D. Dhaygude, B.P. Relekar, G.M. Lohar, V.J. Fulari, Adv. Sci. Lett. **21**, 2590 (2015)
6. B.P. Relekar, S.A. Mahadik, S.T. Jadhav, A.S. Patil, R.R. Koli, G.M. Lohar, V.J. Fulari, J. Electron. Mater. **47**, 2731 (2018)
7. B.P. Relekar, G.M. Lohar, P.S. Indapure, S.T. Punde, S.T. Jadhav, H.D. Dhygude, V.J. Fulari, Mater. Focus **5**, 577 (2016)
8. S.S. Mali, S.K. Shinde, J.R. Mane, A.A. Mane, S.A. Swami, H.D. Dhaygude, G.M. Lohar, B.P. Relekar, V.J. Fulari, Adv. Sci. Lett. **21**, 2594 (2015)
9. J. V. Thombare, G. M. Lohar, S. K. Shinde, U. M. Chougale, V. J. Fulari, A. B. Kadam, S. S. Dhasade, M. C. Rath, and S. H. Han, in *2013 Int. Conf. Energy Effic. Technol. Sustain. ICEETS 2013* (IEEE, 2013), pp. 1064–1067.
10. S. Zhang, H. Gao, J. Zhou, F. Jiang, Z. Zhang, J. Alloys Compd. **792**, 474 (2019)
11. J. Xu, L. Wu, Y. Liu, J. Zhang, J. Liu, S. Shu, X. Kang, Q. Song, D. Liu, F. Huang, Y. Hu, Surf. Interfaces **18**, 100420 (2020)
12. W. Liu, C. Lu, X. Wang, K. Liang, B.K. Tay, J. Mater. Chem. A **3**, 624 (2014)
13. K. Qiu, H. Yan, D. Zhang, Y. Lu, J. Cheng, W. Zhao, C. Wang, Y. Zhang, X. Liu, C. Cheng, Y. Luo, Electrochim. Acta **141**, 248 (2014)
14. W. Huang, S. Ding, Y. Chen, W. Hao, X. Lai, J. Peng, J. Tu, Y. Cao, X. Li, Sci. Rep. **7**, 5220 (2017)
15. M.L. Huang, C.D. Gu, X. Ge, X.L. Wang, J.P. Tu, J. Power Sources **259**, 98 (2014)
16. Y. Bu, S. Wang, H. Jin, W. Zhang, J. Lin, J. Wang, J. Electrochem. Soc. **159**, A990 (2012)
17. T. Rakesh Kumar, C.H. Shilpa Chakra, S. Madhuri, E. Sai Ram, K. Ravi, J. Mater. Sci. Mater. Electron. **32**, 20374 (2021)
18. J. Yus, Y. Bravo, A.J. Sanchez-Herencia, B. Ferrari, Z. Gonzalez, Electrochim. Acta **308**, 363 (2019)
19. O.C. Pore, A.V. Fulari, N.B. Velha, V.G. Parale, H.H. Park, R.V. Shejwal, V.J. Fulari, G.M. Lohar, Mater. Sci. Semicond. Process. **134**, 105980 (2021)
20. A.S. Patil, G.M. Lohar, V.J. Fulari, J. Mater. Sci. Mater. Electron. **27**, 9550 (2016)
21. G.M. Lohar, O.C. Pore, A.V. Fulari, Ceram. Int. **47**, 16674 (2021)
22. Z. Lotfi, M.B. Gholivand, M. Shamsipur, Anal. Biochem. **616**, 114062 (2021)
23. W. Alghazzawi, E. Danish, H. Alnahdi, M.A. Salam, Synth. Met. **267**, 116401 (2020)
24. F. Li, R. Liu, V. Dubovyk, Q. Ran, H. Zhao, S. Komarneni, Food Chem. **384**, 132643 (2022)
25. F. Li, R. Liu, V. Dubovyk, Q. Ran, B. Li, Y. Chang, H. Wang, H. Zhao, S. Komarneni, Food Chem. **366**, 130563 (2022)
26. H. Zhao, B. Li, R. Liu, Y. Chang, H. Wang, L. Zhou, S. Komarneni, Mater. Sci. Eng. C **123**, 111982 (2021)
27. H. Zhao, H. Ma, X. Li, B. Liu, R. Liu, S. Komarneni, Appl. Clay Sci. **200**, 105907 (2021)
28. H. Zhao, B. Liu, Y. Li, B. Li, H. Ma, S. Komarneni, Ceram. Int. **46**, 19713 (2020)
29. H. Zhao, Q. Ran, Y. Li, B. Li, B. Liu, H. Ma, M. Zhang, S. Komarneni, J. Mater. Res. Technol. **9**, 9422 (2020)
30. D. Li, X. Hu, H. Zhao, K. Ding, F. Li, S. Han, H. Wang, L. Bai, R. Liu, J. Porous Mater. **293**(29), 629 (2022)
31. H. Zhang, S. Liu, Sensors Actuators B Chem. **238**, 788 (2017)
32. P. Lu, J. Yu, Y. Lei, S. Lu, C. Wang, D. Liu, Q. Guo, Sensors Actuators B Chem. **208**, 90 (2015)
33. H. Naeimi, Z. Ansarian, Inorganica Chim. Acta **466**, 417 (2017)
34. Z. Wang, Y. Hu, W. Yang, M. Zhou, X. Hu, Sensors **12**, 4860 (2012)
35. A. Kalam, A.G. Al-Sehemi, A.S. Al-Shihri, G. Du, T. Ahmad, Mater. Charact. **68**, 77 (2012)
36. Y.L.T. Ngo, S.H. Hur, Mater. Res. Bull. **84**, 168 (2016)
37. A. Al-Nafiey, A. Kumar, M. Kumar, A. Addad, B. Sieber, S. Szunerits, R. Boukherroub, S.L. Jain, J. Photochem. Photobiol. A Chem. **336**, 198 (2017)
38. Z. Sabouri, N. Fereydouni, A. Akbari, H.A. Hosseini, A. Hashemzadeh, M.S. Amiri, R. Kazemi Oskuee, M. Darroudi, Rare Met. **39**, 1134 (2020)

39. S.D. Khairnar, V.S. Shrivastava, J. Taibah Univ. Sci. **13**, 1108 (2019)
40. O.C. Pore, A.V. Fulari, R.K. Kamble, A.S. Shelake, N.B. Velhal, V.J. Fulari, G. M. Lohar **32**, 20742 (2021)
41. H.T. Das, K. Mahendraprabhu, T. Maiyalagan, P. Elumalai, Sci. Rep. **7**, 15342 (2017)
42. H. Zhu, X. Zeng, T. Han, X. Li, S. Zhu, B. Sun, P. Zhou, J. Liu, J. Solid State Electrochem. **237**(23), 2173 (2019)
43. B.P. Payne, M.C. Biesinger, N.S. McIntyre, J. Electron Spectros. Relat. Phenomena **185**, 159 (2012)
44. G. Zhou, D.W. Wang, L.C. Yin, N. Li, F. Li, H.M. Cheng, ACS Nano **6**, 3214 (2012)
45. O. J. Márquez-Calles, R. D. Martínez-Orozco, N. V Gallardo-Rivas, A. M. Mendoza-Martínez, R. Mayén-Mondragón, U. Páramo-García, de México, and N. León, Int. J. Electrochem. Sci **14**, 5200 (2019).
46. A. Khoshroo, K. Sadrjavadi, M. Taran, A. Fattahi, Sensors Actuators B Chem. **325**, 128778 (2020)
47. C. Zhao, M. M. Thuo, and X. Liu, Sci. Technol. Adv. Mater. **14**, 054402 (2013)
48. N.S. Lopa, M.M. Rahman, F. Ahmed, S.C. Sutradhar, T. Ryu, W. Kim, J. Electroanal. Chem. **822**, 43 (2018)
49. W. Li, Y. Bu, H. Jin, J. Wang, W. Zhang, S. Wang, J. Wang, Energy Fuels **27**, 6304 (2013)
50. V.H. Luan, J.S. Chung, S.H. Hur, RSC Adv. **5**, 22753 (2015)
51. G. Chen, H. Guan, C. Dong, X. Xiao, Y. Wang, J. Phys. Chem. Solids **98**, 209 (2016)
52. X. Feng, J. Zhou, L. Wang, Y. Li, Z. Huang, S. Chen, Y. Ma, L. Wang, X. Yan, New J. Chem. **39**, 4026 (2015)